Supporting Information for:

NMR-Enhanced Crystallography Aids Open Metal-Organic Framework Discovery Using Solvent-Free Accelerated Aging

Christopher A. O'Keefe,[a,†] Cristina Mottillo,[b] Jogirdas Vainauskas,[b] László Fábián,[c] Tomislav Friščić[b,*] and Robert W. Schurko[d,*]

[a] Department of Chemistry and Biochemistry, University of Windsor, Windsor, ON, Canada, N9B 3P4;

[b] Department of Chemistry, McGill University, Montreal, QC, Canada, H3A 0B8;

[c] School of Pharmacy, University of East Anglia, Norwich, UK, NR4 7TJ

[d] Department of Chemistry and Biochemistry, Florida State University, Tallahassee, FL, 32308

[†]Current address: Department of Chemistry, University of Cambridge, Cambridge, UK, CB2 1EW

*Authors to whom correspondence should be addressed:

tomislav.friscic@mcgill.ca

rschurko@fsu.edu

Table of Contents **pg.**

Table S1: Optimized recycle delays for ^{1}H MAS experiments

Compound	Recycle Delay (s)
1	5
2	5
3	5
4	7.5

Table S2: ^{1}H-^{13}C CP/MAS contact times and recycle delays

Compound	Contact Time (ms)	Recycle Delay (s)
1	1	5
2	10	5
3	2	5
4	2	7.5
HMeIm	15	60

Table S3: ^{1}H-^{111}Cd CP contact times and recycle delays

Compound	Contact Time (ms)	Recycle Delay (s)
1	8	5
2	17	5
3	7	5
4	5	7.5

Table S4: ^{1}H-^{14}N BRAIN-CP/WURST-CPMG experimental parameters

Compound	Recycle Delay (s)	Contact Time (ms)	# of echoes	# of subspectra
1	1	20	40	15
HMeIm	30	20	80	26

Table S5: Selected bond lengths in the Cd-imidazole compounds with known structures

Compound	Bond	Length (Å)
2	Cd-N1	2.215
	Cd-N2	2.228
	Cd-N3	2.260
	Cd-N4	2.226
3	Cd1-N2	2.203
	Cd1-N3	2.198
	Cd1-N5	2.199
	Cd1-N6	2.258
	Cd1-N7	2.167
	Cd2-N1	2.201
	Cd2-N2	2.209
4	Cd-N1	2.401

Table S6: Selected bond angles in the Cd-imidazole compounds with known structures

Compound	Bond	Angle (°)
2	N1-Cd-N2	113.5
	N1-Cd-N3	115.2
	N1-Cd-N4	112.2
	N2-Cd-N3	96.66
	N2-Cd-N4	112.9
	N3-Cd-N4	105.3
3	N2-Cd1-N3	115.3
	N2-Cd1-N5	115.6
	N2-Cd1-N6	80.97
	N2-Cd1-N7	107.4
	N3-Cd1-N5	109.9
	N3-Cd1-N6	126.1
	N3-Cd1-N7	102.0
	N5-Cd1-N6	106.5
	N5-Cd1-N7	105.1
	N6-Cd1-N7	29.33
	N1-Cd2-N2	106.8
	N1-Cd2-N2	117.4
4	N1-Cd-N1	89.769
	N1-Cd-N1	90.231

2. Solid-state NMR data

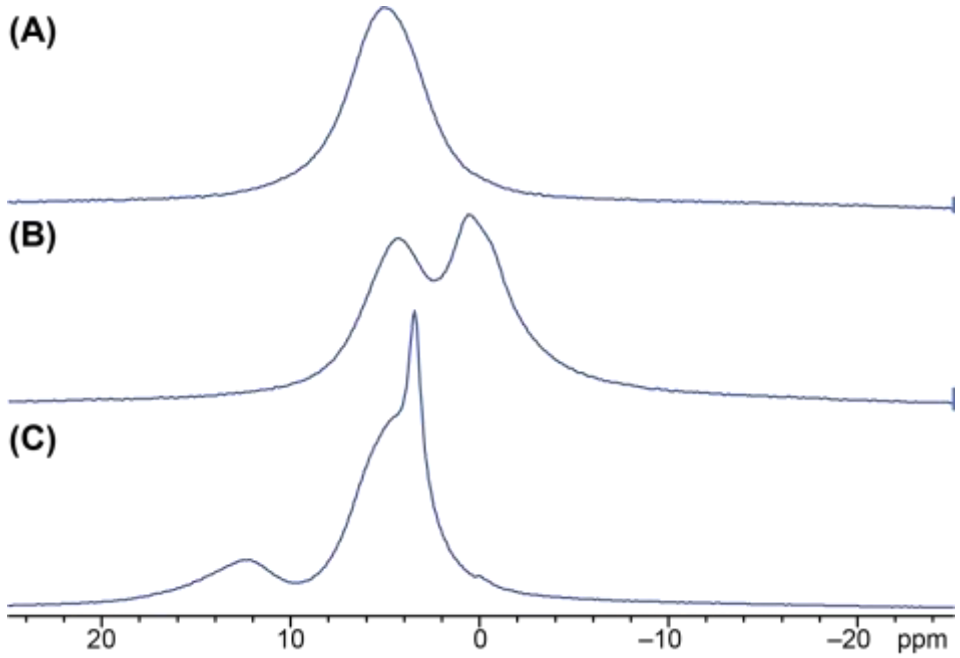

Figure S1: ^{1}H MAS (ν_{rot} = 16 kHz) NMR spectra acquired at 9.4 T for (**A**) framework **2**, (**B**) framework **3**, and (**C**) compound **4**.

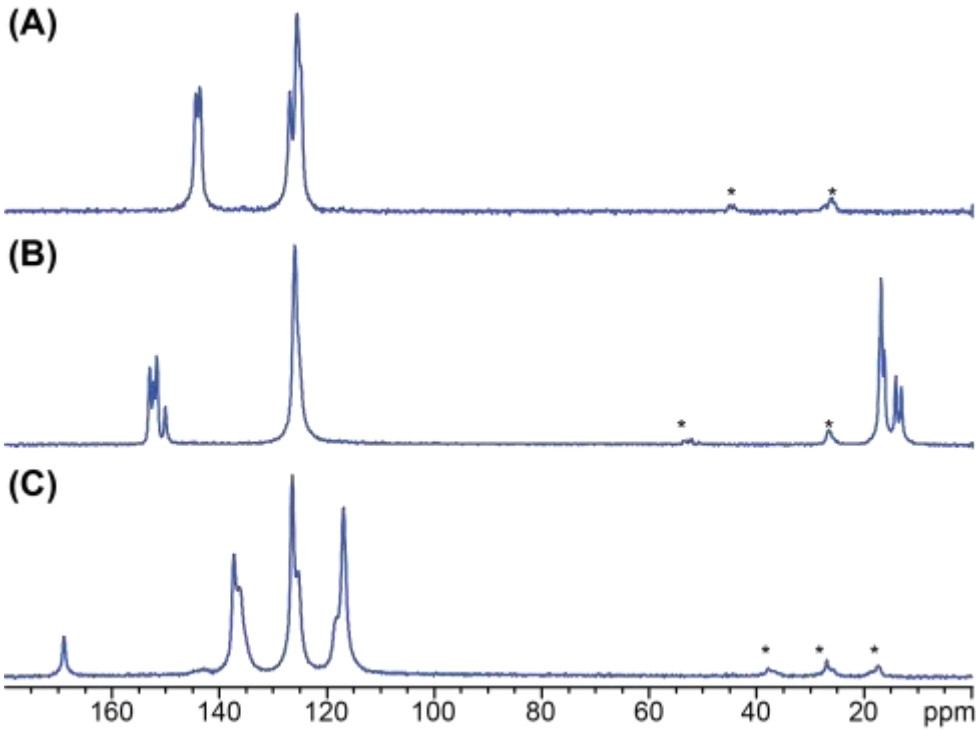

Figure S2: ^{1}H-^{13}C CP/MAS (ν_{rot} = 10 kHz) NMR spectra acquired at 9.4 T of (**A**) framework **2**, (**B**) framework **3**, and **(C**) compound **4**. The asterisks (*) denoted spinning sidebands.

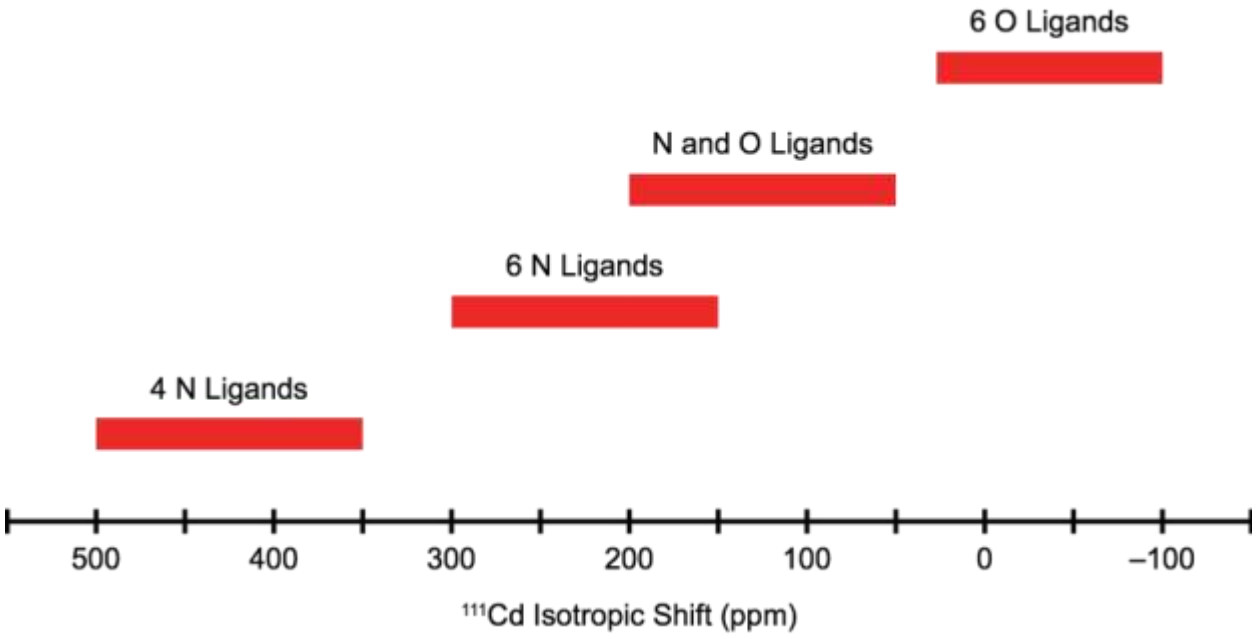

Figure S3: Proposed ^{111}Cd isotropic chemical shift ranges based on the compounds investigated herein and on studies conducted by Ellis *et al.*[17–24] and Baxter *et al.*[25]

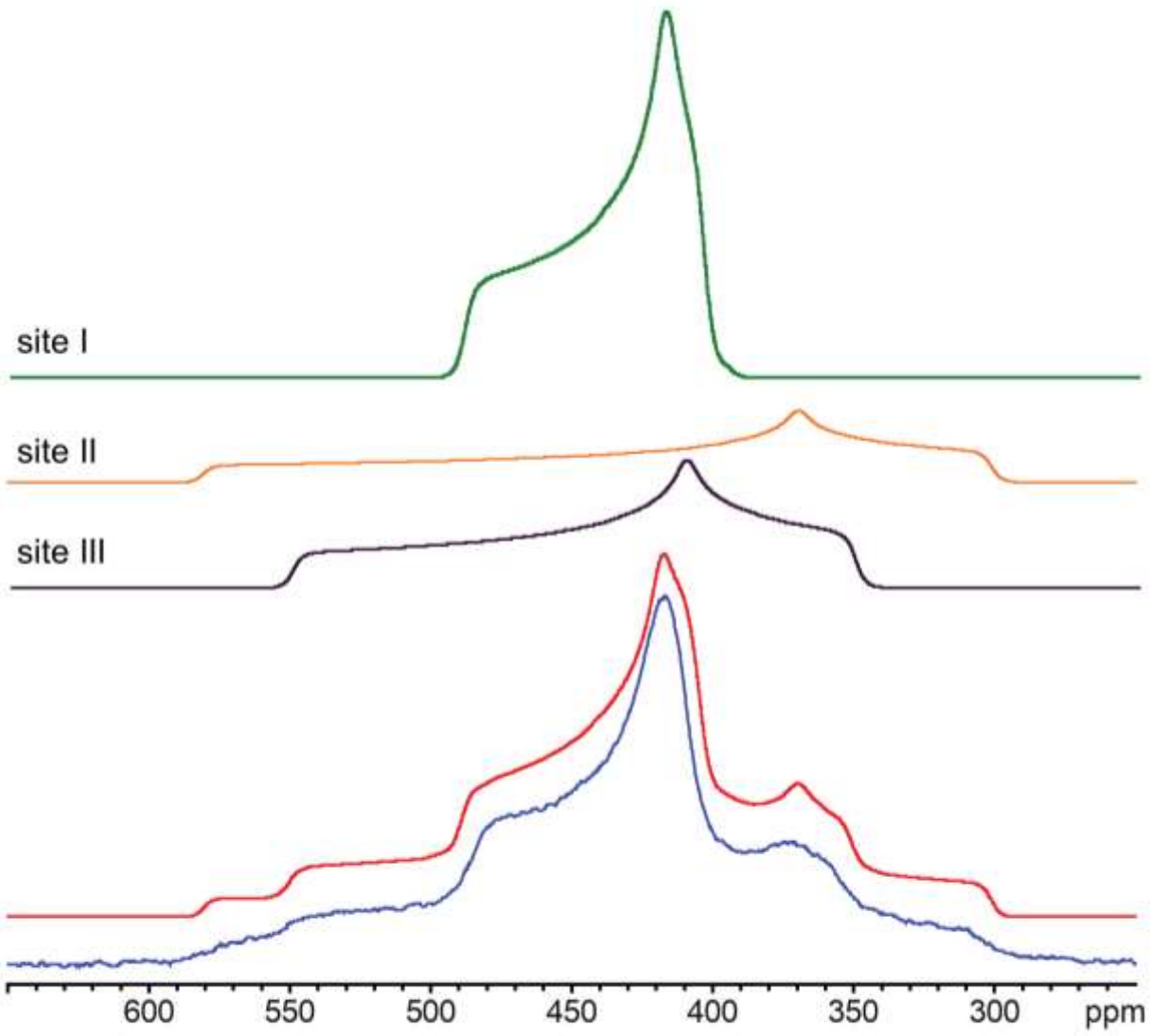

Figure S4: Experimental ^{1}H-^{111}Cd CP static spectrum of **2** (blue trace). Simulation of the entire spectrum is shown in the red trace. The simulation is deconvoluted into the individual sites: site I (green trace), site II (orange trace), and site III (black trace). The corresponding ^{111}Cd CS tensor parameters can be found in **Table 1** in the main text.

^{1}H-^{14}N BRAIN-CP/WURST-CPMG

The ^{1}H-^{14}N static CP NMR spectra for H**MeIm** and **1** are shown in **Figure S5**. Due to the enormous breadth (*ca.* 4.5 MHz) of ^{14}N patterns, it was necessary to use the broadband adiabatic inversion CP (BRAIN-CP) for polarization transfer,[3,4] and the wideband uniform-rate smooth-truncation-CPMG (WURST-CPMG) pulse sequence for broadband refocusing.[5,6,26] The spectrum of bulk H**MeIm** reveals two overlapping Pake-like doublet patterns, corresponding to two distinct nitrogen environments (**Figure S6**). The narrower pattern (C_Q = 1.95(5) MHz, η_Q = 0.44(2)) is assigned to the nitrogen of the N-H group and the broader pattern (C_Q = 3.13(5), η_Q = 0.21(2)) to the non-protonated nitrogen atom. The spectrum of **1** exhibits several broad features resulting from multiple overlapping Pake doublet patterns. Some of the features (*i.e.*, horns, shoulders, and feet) in the spectrum of **1** occur at the same frequency as those for bulk H**MeIm**, consistent with H**MeIm** inclusion in the MOF. Furthermore, discontinuities in the spectrum of **1** are not as well defined as those for bulk H**MeIm**, suggesting that guest molecules are disordered in the former. Finally, there are discontinuities in the ^{14}N spectrum of **1** that do not match those in the spectrum of **HMeIm**; these are assigned to nitrogen atoms of **MeIm**$^{-}$ ligands forming the framework of **1**.

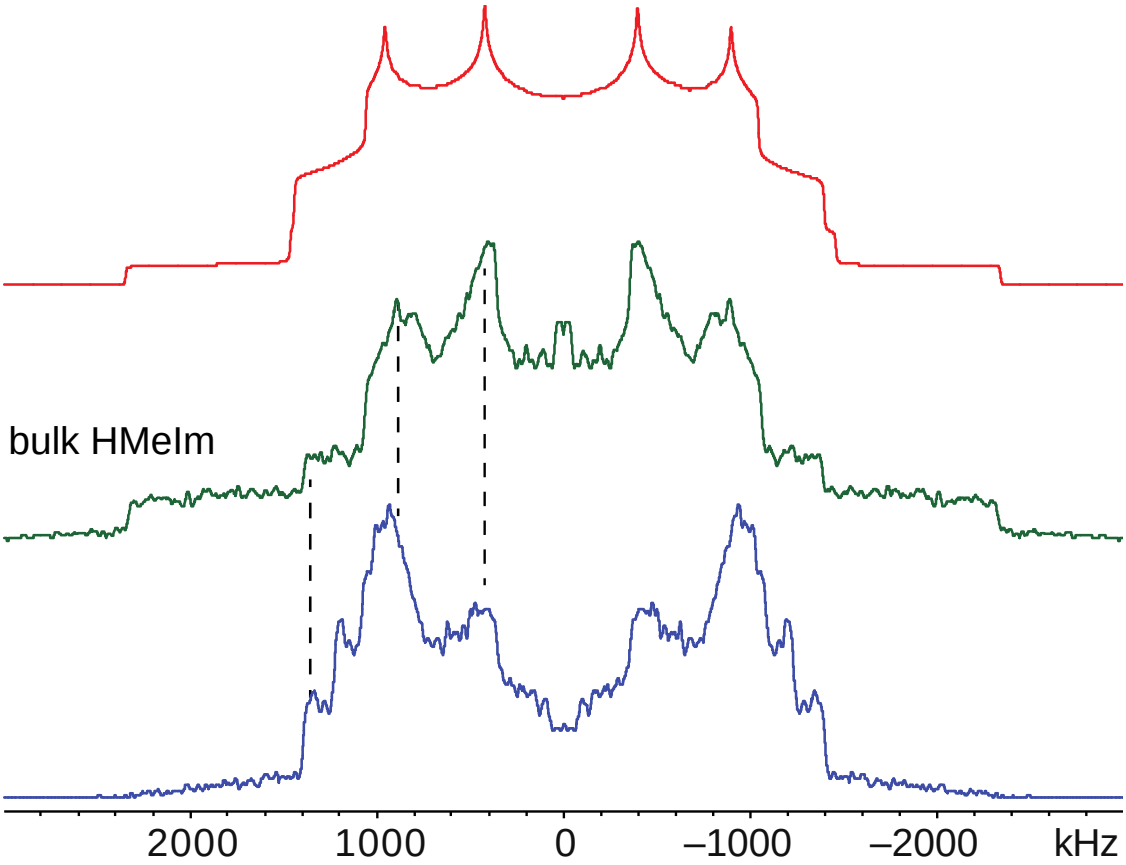

Figure S5: ^{1}H-^{14}N BRAIN-CP/WURST-CPMG spectra of H**MeIm** (green trace) and **1** (blue trace).

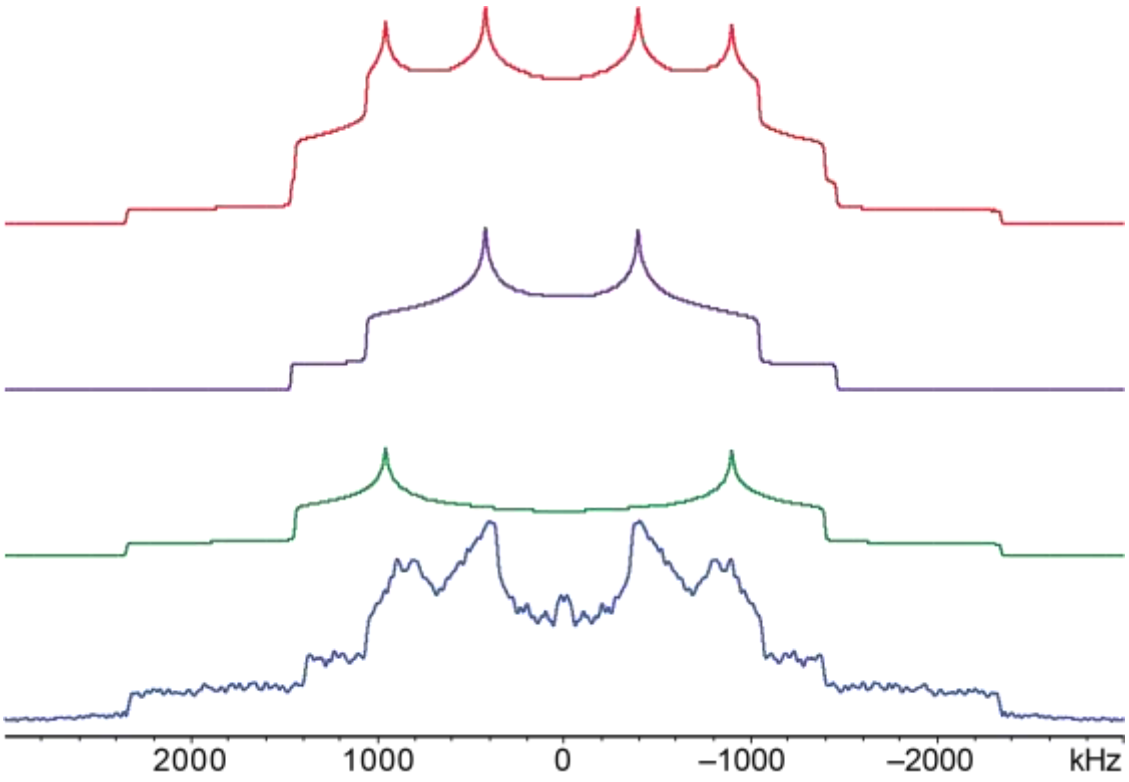

Figure S6: ^{1}H-^{14}N BRAIN-CP/WURST-CPMG spectrum of bulk **HMeIm** (blue trace) and simulation of the powder pattern (red trace). A deconvolution of the simulation into the two distinct powder patterns is also shown. The purple trace is the pattern corresponding to the N1 site (C_Q = 1.95(5) MHz, η_Q = 0.44(2)) and the green trace is the pattern corresponding to the N2 site (C_Q = 3.13(5) MHz, η_Q = 0.21(2)).

3. Powder X-ray diffraction data

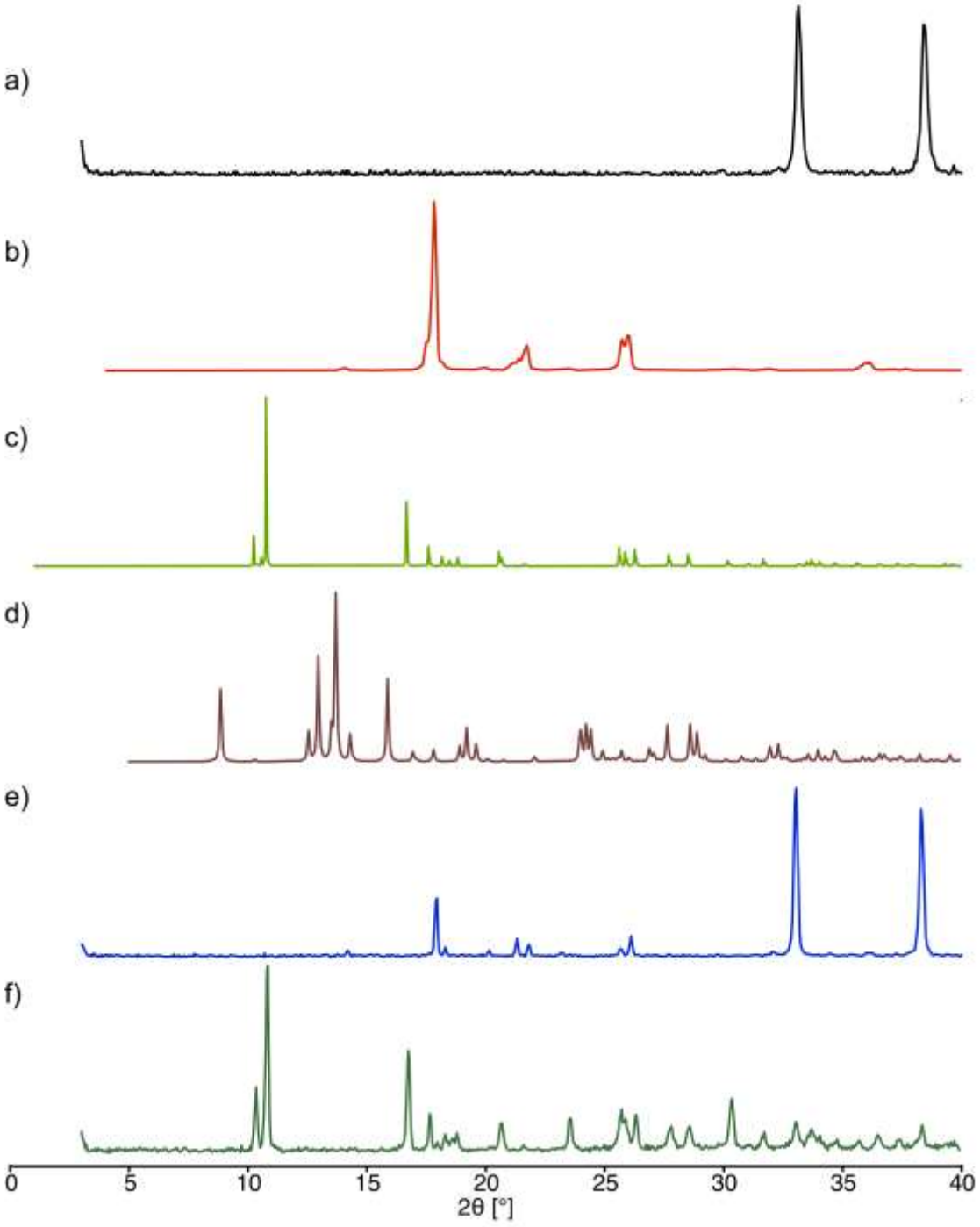

Figure S7: Experimental PXRD patterns of: a) commercial CdO; b) commercial H**MeIm**; c) simulated PXRD pattern for herein reported compound **1**; d) simulated PXRD pattern of **yqt1**-Cd(**MeIm**)$_2$ (CSD code GUPBOJ) (**3**); experimental PXRD patterns of a 1:2 stoichiometric mixture of CdO and H**MeIm** after: e) pre-milling for 5 min at 30 Hz, and f) aging at 45 C and 100% RH for 12 days.

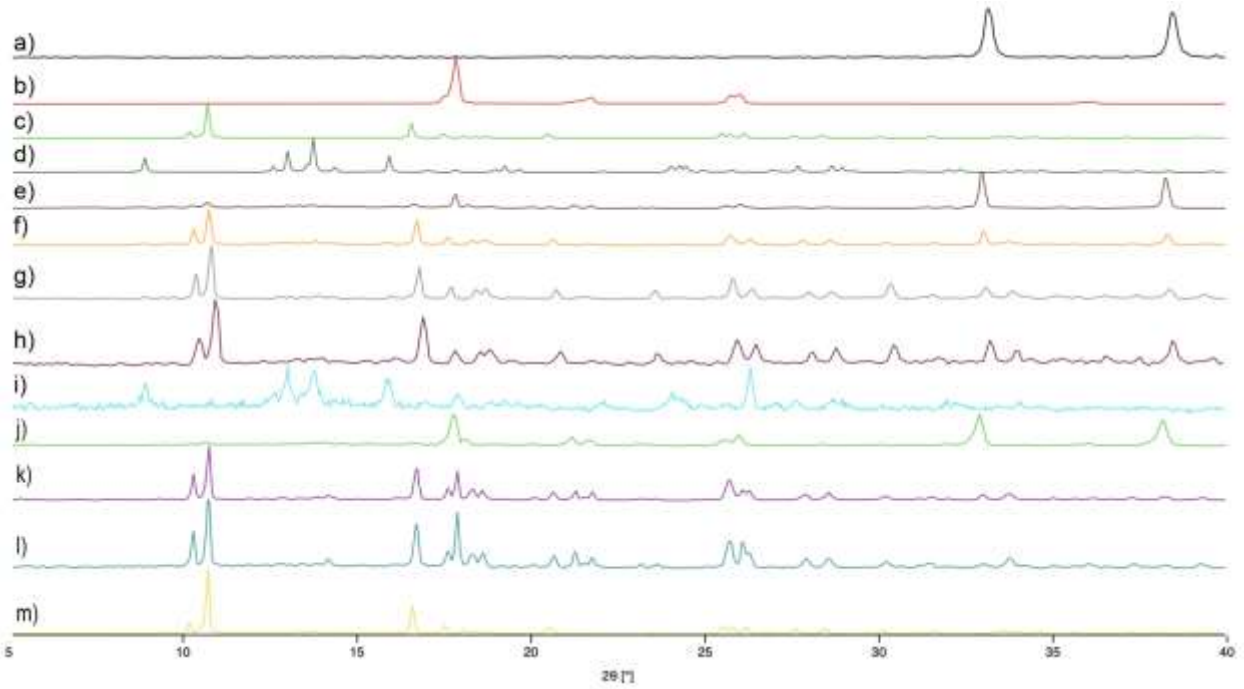

Figure S8: Experimental PXRD patterns of: a) commercial CdO; b) commercial H**MeIm**; simulated PXRD patterns of: c) **dia**-Cd(**MeIm**)$_2$·H**MeIm** (**1**), and d) **yqt1**-Cd(**MeIm**)$_2$ (CSD code GUPBOJ) (**3**); experimental PXRD patterns of a 1:2 stoichiometric mixture of CdO and H**MeIm** in the presence of NH_4NO_3 after: e) pre-milling for 5 min at 30 Hz; aging at 45 °C and 100% RH for: f) 1 day, g) 7 days, and h) 7 months; i) sample g) after heating to 200 °C; experimental PXRD patterns of a 1:6 stoichiometric mixture of CdO and H**MeIm** in the presence of NH_4NO_3 after: j) pre-milling for 5 min at 30 Hz; aging at 45 °C and 100% RH for: k) 3 days, and l) 7 days; m) experimental PXRD patterns of a 1:3 stoichiometric mixture of CdO and H**MeIm** in the presence of NH_4NO_3 after aging at 45 °C and 100% RH for 4 days.

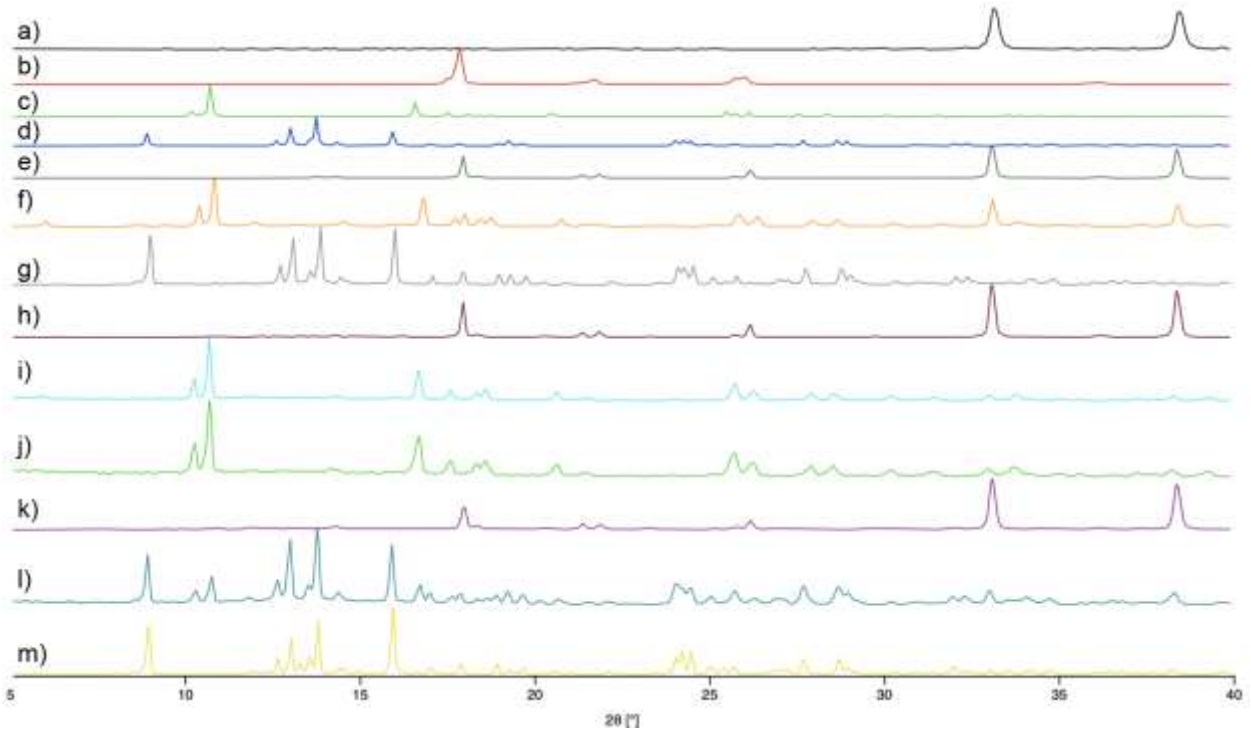

Figure S9: Experimental PXRD patterns of: a) commercial CdO; b) commercial H**MeIm**; simulated PXRD patterns of: c) **dia**-Cd(**MeIm**)$_2$·H**MeIm** (**1**), and d) **yqt1**-Cd(**MeIm**)$_2$ (CSD code GUPBOJ) (**3**); experimental PXRD patterns of a 1:2 stoichiometric mixture of CdO and H**MeIm** in the presence of $(NH_4)_2SO_4$ after: e) pre-milling for 5 min at 30 Hz; aging at 45 °C and 100% RH for: f) 1 day, and g) 7 days; experimental PXRD patterns of a 1:3 stoichiometric mixture of CdO and H**MeIm** in the presence of $(NH_4)SO_4$ after: h) pre-milling for 5 min at 30 Hz; aging at 45 °C and 100% RH for: i) 4 days, and j) 6 days; experimental PXRD patterns of a 1:2 stoichiometric mixture of CdO and H**MeIm** in the presence of H**Caf**HSO_4 after: k) pre-milling for 5 min at 30 Hz; aging at 45 °C and 100% RH for: l) 1 day, and m) 7 days.

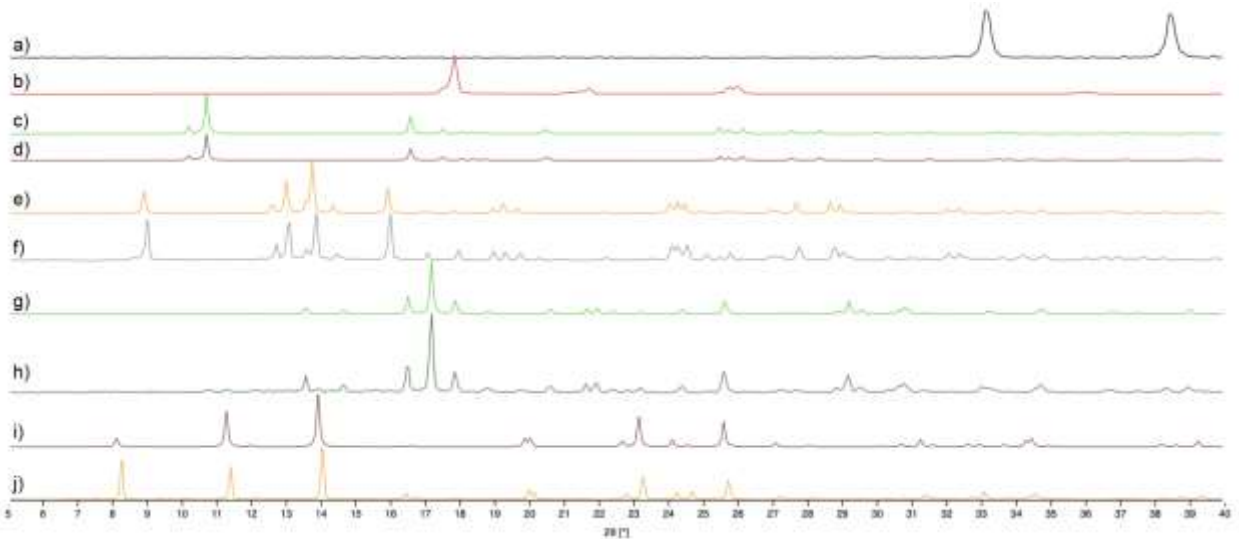

Figure S10: Experimental PXRD patterns of: a) commercial CdO; b) commercial H**MeIm**; c) simulated, and d) experimental PXRD pattern of **dia**-Cd(**MeIm**)$_2$·H**MeIm** (**1**); e) simulated, and f) experimental PXRD pattern of **yqt1**-Cd(**MeIm**)$_2$ (CSD code GUPBOJ) (**3**); g) simulated, and h) experimental PXRD pattern of **dia**-Cd(**Im**)$_2$ (CSD code BAYQAU) (**2**); i) simulated, and j) experimental PXRD pattern of Cd(H**Im**)$_6$CO$_3$·3H$_2$O (CSD code IMIDCP01) (**4**).

4. Thermogravimetric analysis

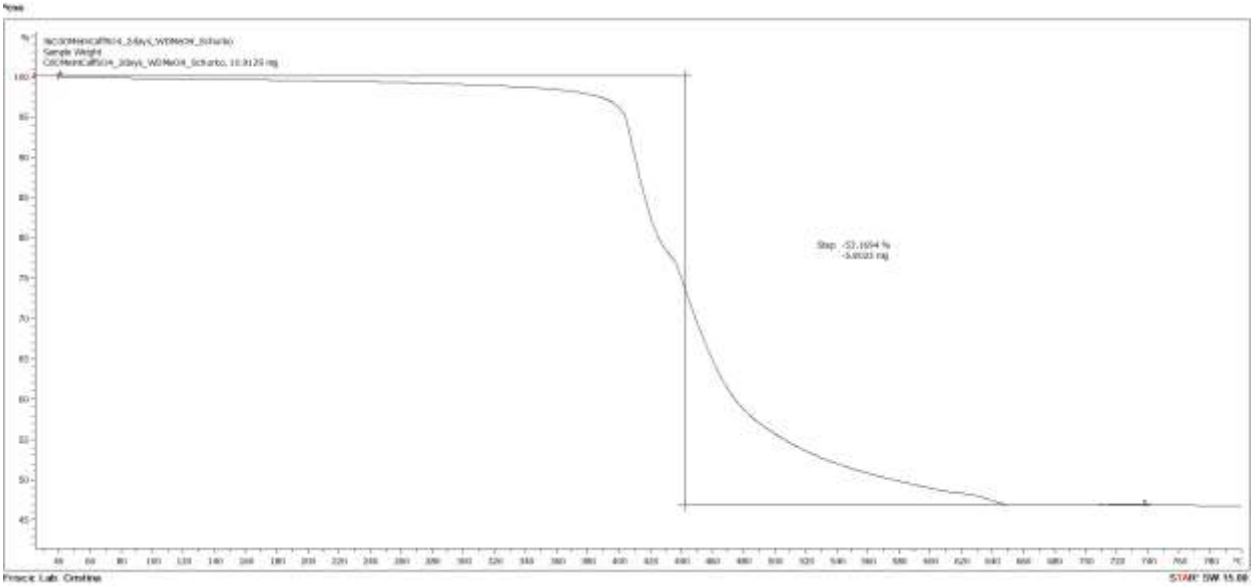

Figure S11: TGA thermogram of **yqt1**-Cd(**Im**)$_2$ (CSD code GUPBOJ) (**3**) in a dynamic atmosphere of air. The sample was made by aging CdO and H**MeIm** in a 1:2 ratio at 45 °C and 100% RH in the presence of (H**Caf**)HSO_4.

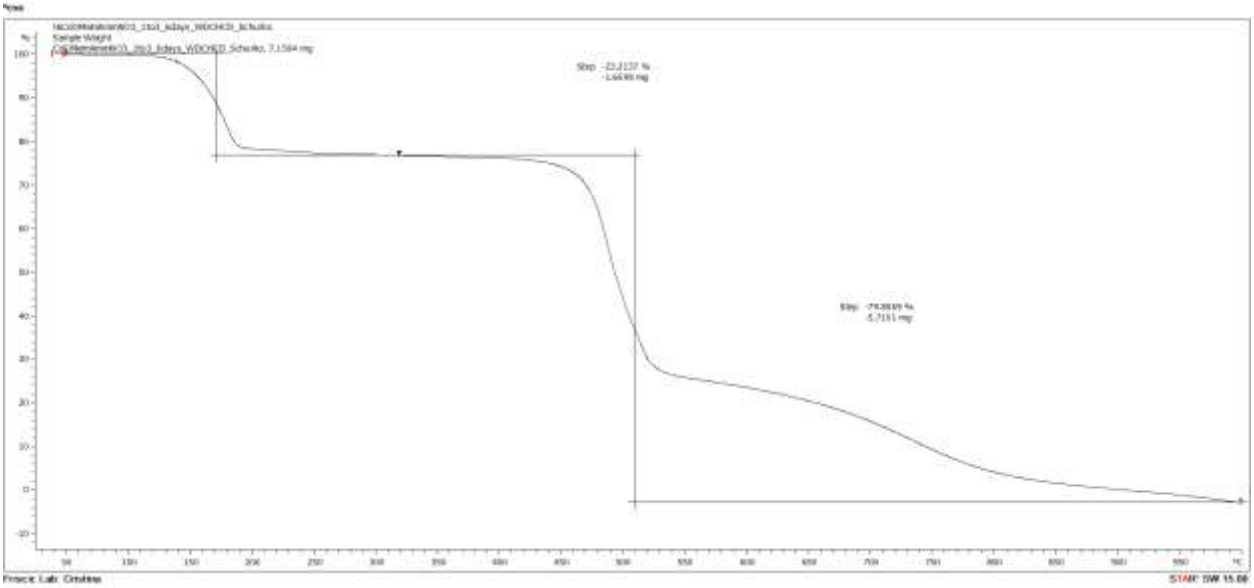

Figure S12: TGA thermogram of **dia**-Cd(**MeIm**)$_2$·H**MeIm** (**1**) in a dynamic atmosphere of N_2. The first step corresponds to the loss of one molecule of unbound H**MeIm** per Cd^{2+}, which accounts for a theoretical value of 23.03% w/w of **1** (experimental value is 23.21%).

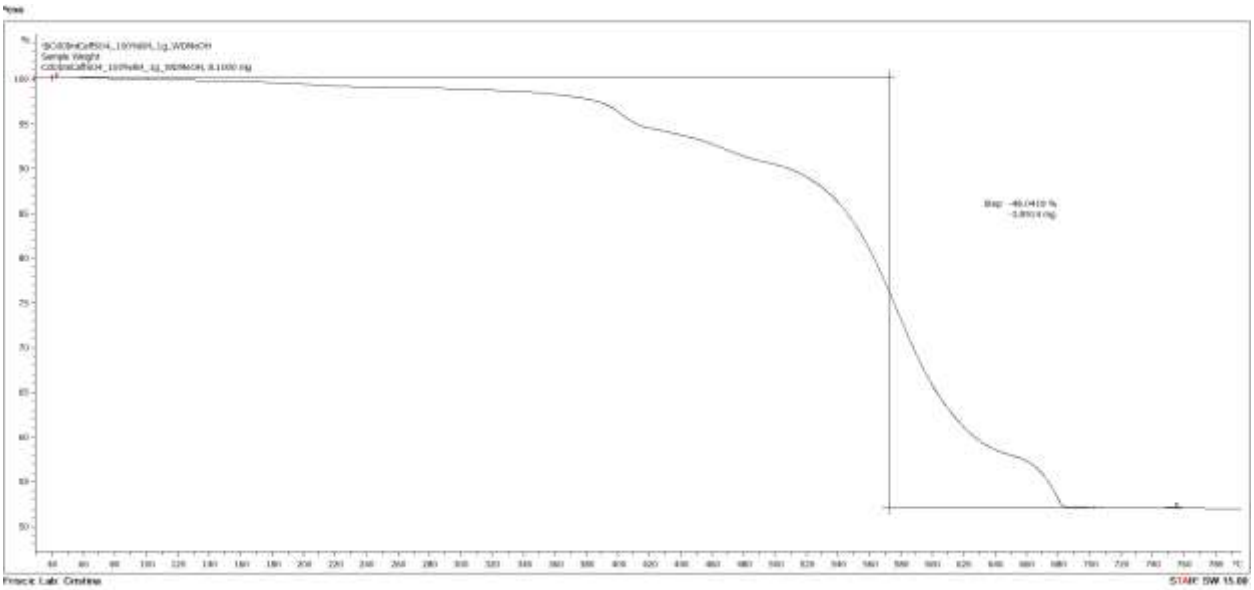

Figure S13: TGA thermogram of **dia**-Cd(**Im**)$_2$ (CSD code BAYQAU) (**2**) in a dynamic atmosphere of air.

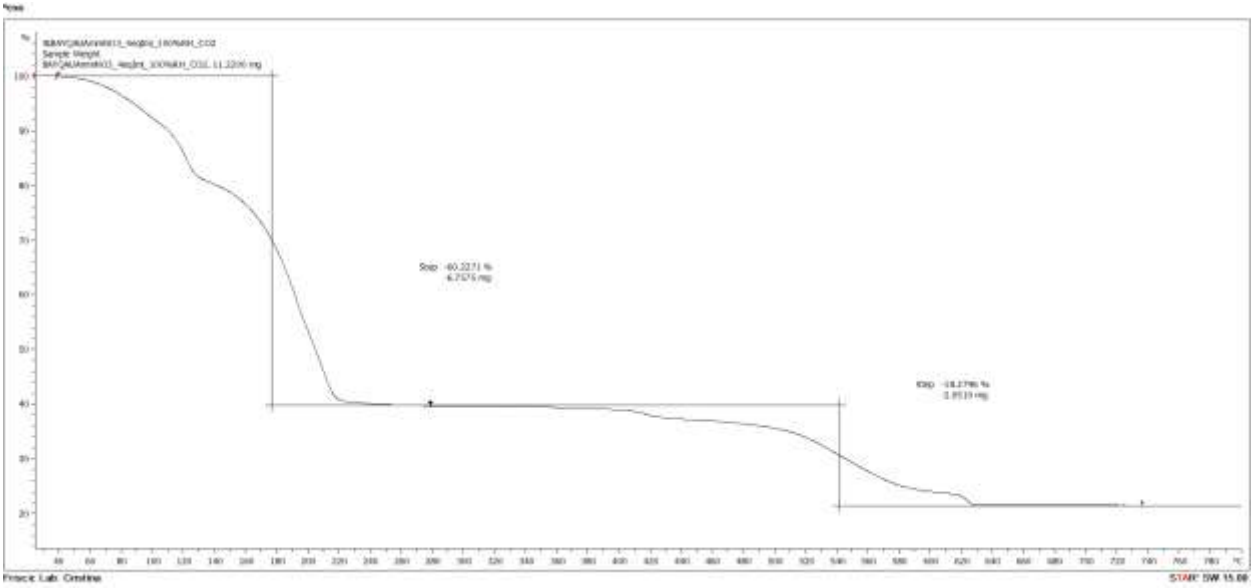

Figure S14: TGA thermogram of Cd(H**Im**)$_6$·3H$_2$O (CSD code IMCDCP01) (**4**) in a dynamic atmosphere of air.

4. Fourier-transform infrared (FTIR-ATR) spectroscopy

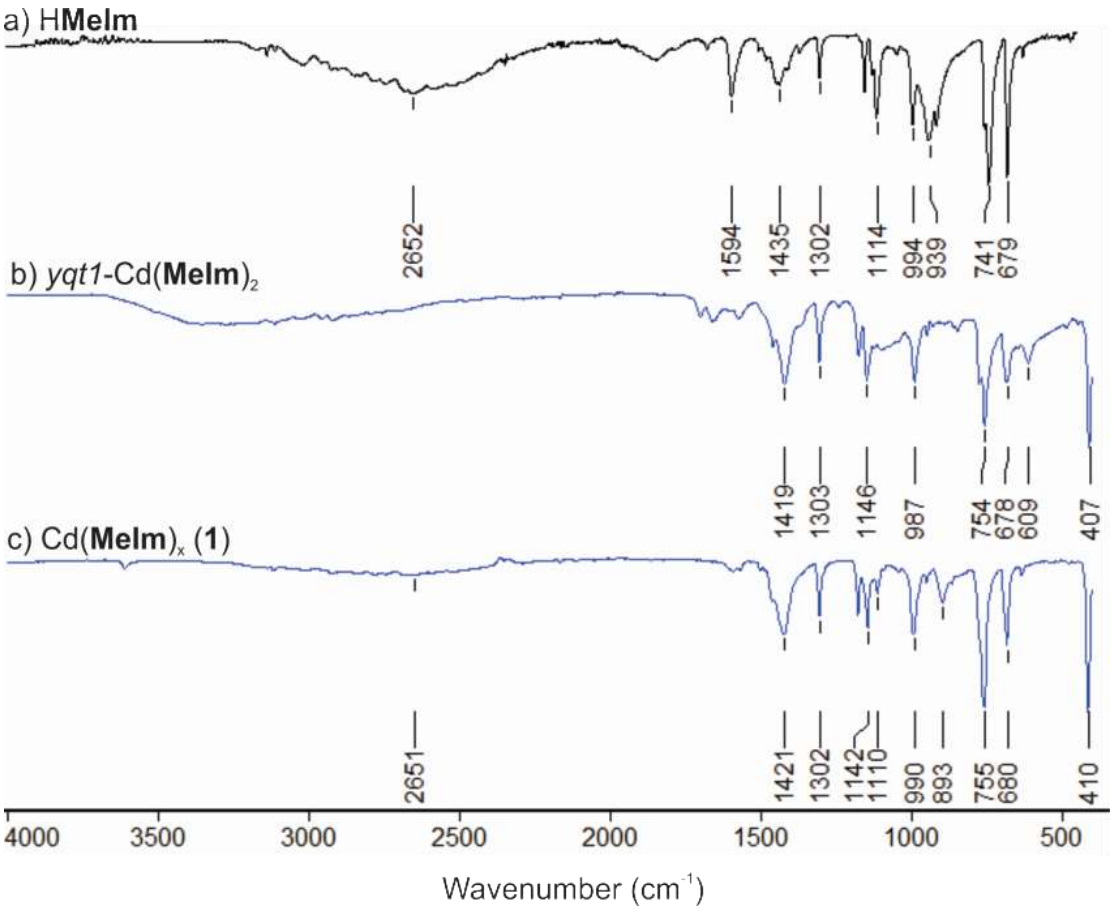

Figure S15: Fourier-transform infrared (FTIR-ATR) spectra of: a) commercial H**MeIm**; b) **yqt1**-Cd(**MeIm**)$_2$ (CCDC code GUPBOJ) (**3**); and c) **dia**-Cd(**MeIm**)$_2$·H**MeIm** (**1**).

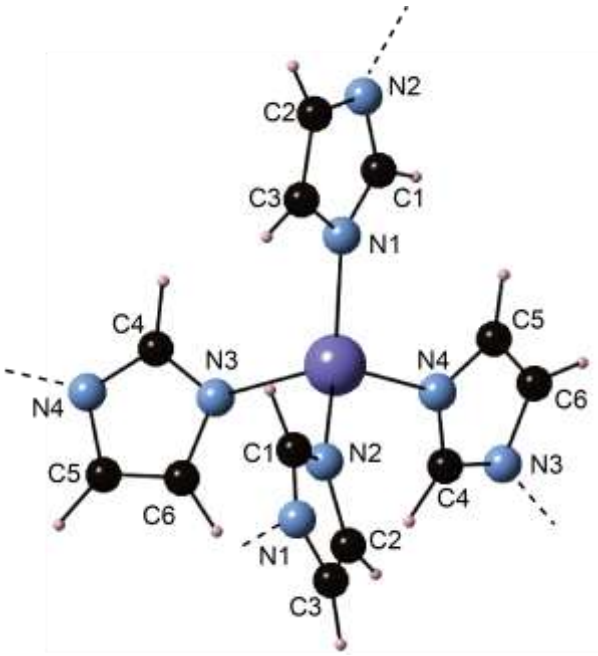

Figure S16: The coordination environment of the Cd atoms in **dia**-Cd[Im]$_2$ (**2**).

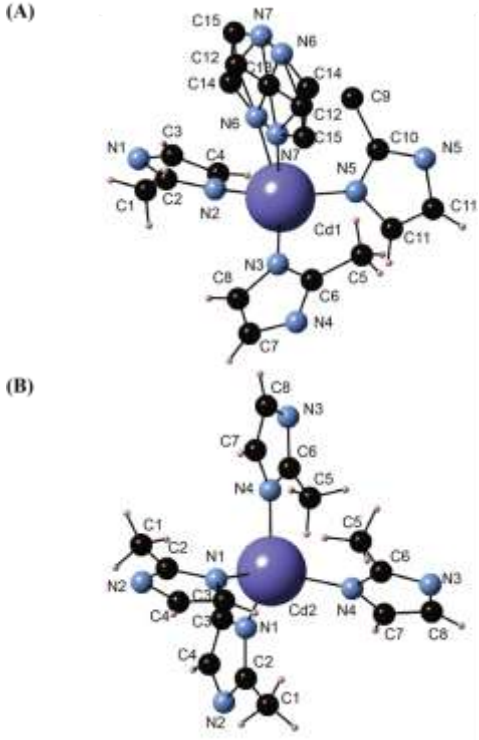

Figure S17: Coordination environment about (**A**) the Cd1 site, (**B**) the Cd2 site and atom labeling in the **yqt1**-Cd[MeIm]$_2$ (**3**) framework. There is an apparent positional disorder of one of the MeIm$^-$ ligands at the Cd1 site.

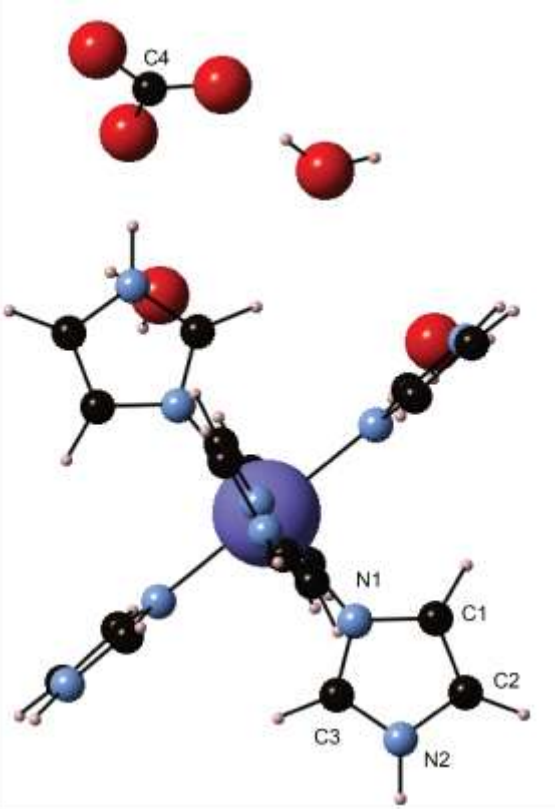

Figure S18: Coordination environment about the Cd atom and atom labelling in the $Cd[Im]_6CO_3 \cdot 3H_2O$ (**4**) molecule.

References:

[1] C. Mottillo, Y. Lu, M.-H. Pham, M. J. Cliffe, T.-O. Do, T. Friščić, *Green Chem.* **2013**, *15*, 2121.

[2] O. B. Peersen, X. Wu, I. Kustanovich, S. O. Smith, *J. Magn. Reson. Ser. A* **1993**, *104*, 334–339.

[3] K. J. Harris, A. Lupulescu, B. E. G. Lucier, L. Frydman, R. W. Schurko, *J. Magn. Reson.* **2012**, *224*, 38–47.

[4] K. J. Harris, S. L. Veinberg, C. R. Mireault, A. Lupulescu, L. Frydman, R. W. Schurko, *Chem. Eur. J.* **2013**, *19*, 16469–16475.

[5] L. A. O'Dell, R. W. Schurko, *Chem. Phys. Lett.* **2008**, *464*, 117–130.

[6] L. A. O'Dell, A. J. Rossini, R. W. Schurko, *Chem. Phys. Lett.* **2009**, *468*, 330–335.

[7] D. Massiot, I. Farnan, N. Gautier, D. Trumeau, A. Trokiner, J. P. Coutures, *Solid State Nucl. Magn. Reson.* **1995**, *4*, 241–8.

[8] A. Medek, V. Frydman, L. Frydman, *J. Phys. Chem. A* **1999**, *103*, 4830–4835.

[9] J. A. Tang, J. D. Masuda, T. J. Boyle, R. W. Schurko, *ChemPhysChem* **2006**, *7*, 117–30.

[10] S. L. Veinberg, Z. W. Friedl, K. J. Harris, L. A. O'Dell, R. W. Schurko, *CrystEngComm* **2015**, *17*, 5225–5236.

[11] S. L. Veinberg, Z. W. Friedl, A. W. Lindquist, B. Kispal, K. J. Harris, L. A. O'Dell, R. W. Schurko, *ChemPhysChem* **2016**, *17*, 4011–4027.

[12] S. L. Veinberg, K. E. Johnston, M. J. Jaroszewicz, B. M. Kispal, C. R. Mireault, T. Kobayashi, M. Pruski, R. W. Schurko, *Phys. Chem. Chem. Phys.* **2016**, *18*, 17713–17730.

[13] A. Le Bail, *Powder Diffr.* **2004**, *19*, 249–254.

[14] W. I. F. David, K. Shankland, J. van de Streek, E. Pidcock, W. D. S. Motherwell, J. C.

Cole, *J. Appl. Crystallogr.* **2006**, *39*, 910–915.

[15] A. C. Larson, R. Von Dreele, *General Structure Analysis System (GSAS)*, **2004**.

[16] B. H. Toby, *J. Appl. Crystallogr.* **2001**, *34*, 210–213.

[17] H. J. Jakobsen, P. D. Ellis, R. R. Inners, C. F. Jensen, *J. Am. Chem. Soc.* **1982**, *104*, 7442–7452.

[18] M. A. Kennedy, P. D. Ellis, H. J. Jakobsen, *Inorg. Chem.* **1990**, *29*, 550–552.

[19] M. A. Kennedy, J. L. Sessler, T. Murai, P. D. Ellis, H. J. Jakobsen, *Inorg. Chem.* **1990**, *29*, 1050–1054.

[20] E. Rivera, M. A. Kennedy, R. D. Adams, P. D. Ellis, *J. Am. Chem. Soc.* **1990**, *112*, 1400–1407.

[21] E. Rivera, P. D. Ellis, *Inorg. Chem.* **1992**, *11*, 2096–2103.

[22] A. S. Lipton, S. S. Mason, D. L. Reger, P. D. Ellis, *J. Am. Chem. Soc.* **1994**, *116*, 10182–10187.

[23] D. L. Reger, S. M. Myers, S. S. Mason, D. J. Darensbourg, M. W. Holtcamp, J. H. Reibenspies, A. S. Lipton, P. D. Ellis, *J. Am. Chem. Soc.* **1995**, *117*, 10998–11005.

[24] A. S. Lipton, S. S. Mason, S. M. Myers, D. L. Reger, P. D. Ellis, **1996**, *2*, 7111–7117.

[25] E. F. Baxter, T. D. Bennett, A. B. Cairns, N. J. Brownbill, A. L. Goodwin, D. A. Keen, P. A. Chater, F. Blanc, A. K. Cheetham, *Dalt. Trans.* **2016**, *45*, 4258–4268.

[26] L. A. O'Dell, *Solid State Nucl. Magn. Reson.* **2013**, *55–56*, 28–41.